Band structure of twisted bilayer graphene on hexagonal boron nitride

Tommaso Cea [1,2,*] Pierre A. Pantaleón [2,*] and Francisco Guinea [2,3]

[1] *Instituto de Ciencia de Materiales de Madrid, CSIC, Sor Juana Inés de la Cruz 3, Cantoblanco, 28049 Madrid, Spain*

[2] *Imdea Nanoscience, Faraday 9, 28015 Madrid, Spain*

[3] *Donostia International Physics Center, Paseo Manuel de Lardizábal 4, 20018 San Sebastián, Spain*

(Received 19 May 2020; revised 12 August 2020; accepted 6 October 2020; published 23 October 2020)

The effect of a hexagonal boron nitride (hBN) layer closely aligned with twisted bilayer graphene (TBG) is studied. At sufficiently low angles between twisted bilayer graphene and hBN, $\theta_{hBN} \lesssim 2^\circ$, the graphene electronic structure is strongly disturbed. The width of the low-energy peak in the density of states changes from $W \sim$ 5–10 meV for a decoupled system to ∼20–30 meV. Spikes in the density of states due to van Hove singularities are smoothed out. We find that for a realistic combination of the twist angle in the TBG and the twist angle between the hBN and the graphene layer the system can be described using a single moiré unit cell.

DOI: 10.1103/PhysRevB.102.155136

I. INTRODUCTION

The discovery of insulating behavior at integer filling and superconductivity in twisted bilayer graphene (TBG) [1–5] motivated a recent effort in the study of a wide class of van der Waals heterostructures, displaying moiré patterns on length scales much larger than the lattice constant of their constituent layers. The periodicity induced by the moiré can affect sensitively the electronic structure of the material, giving rise to narrow, almost dispersionless flat bands. The kinetic quenching may favor the interactions between the electrons, paving the way for the appearance of strongly correlated phases.

So far, transport measurements on TBG have been performed with the sample either encapsulated between two hexagonal boron nitride (hBN) clapping layers, see, e.g., [1,2,6–10], or suspended on a substrate of hBN [11,12]. Recently, it has been observed [13] that the presence of an additional layer of WS_2 between hBN and TBG stabilizes the superconductivity phase in a range of angles wider than reported previously. The presence of hBN breaks the in-plane twofold rotational symmetry ($\mathcal{C}_2$), gapping out the Dirac crossing of monolayer graphene [14–26]. Placing TBG on top of hBN accounts for two coexisting moiré patterns: that induced by the mismatch between the lattice constants of hBN and graphene [27–31], and that induced by the relative orientation between the two graphene layers of the TBG. If the hBN is aligned with the adjacent graphene layer and the relative twist between the two layers of graphene is close to 1°, then the two moirés have very similar periods, ∼13 nm, even if they are not commensurate. This sensitively affects the band structure of TBG close to charge neutrality (CN). To a first approximation, it is expected that the breaking of inversion symmetry induced by the hBN layer gives rise to a gap at the Dirac point of the TBG, separating two flat conduction and valence bands, carrying opposite Chern numbers, $\mathcal{C} = \pm 1$ [32,33]. This analysis may explain the observed anomalous Hall effect at the integer band filling, $\nu = 3$ [8,34,35]. The existence of flat bands can lead to Chern insulators, with features similar to those found in the quantum Hall effect [36,37].

In the following, we assume that the twist angle, θ_{TBG}, in the TBG is fixed to a value near a magic angle, and study the effect of a hBN layer as function of the angle between this layer and the neighboring graphene layer, θ_{hBN}. The periodicities of the two moiré patterns described above are $L_{TBG} \approx d_G/\theta_{TBG}$ and $L_{G,hBN} \approx d_G/\sqrt{\theta_{hBN}^2 + (d_{hBN}/d_G)^2}$, where d_G and d_{hBN} are the lattice constants of graphene and hBN. The overall structure resembles the arrangement in a twisted graphene trilayer, or in twisted graphite [38–40]. The two moiré lattices define a generically incommensurate superstructure.

Interestingly, a realistic choice of parameters allows us to define a single moiré unit cell for the whole system. This possibility permits an accurate study of the electronic properties. Interaction effects are included using the unrestricted Hartree-Fock approximation [41]. We analyze the similarities and differences with the electronic structure of TBG decoupled from the substrate, and also with other graphitic systems which show narrow bands [42].

II. THE MODEL

A sketch of the atomic arrangement to be considered and of its Brillouin zone (BZ) is shown in Fig. 1. We assume, as in the continuum model for TBG [43,44], that one side of the hexagonal Brillouin zone of the superlattice connects the corners of the Brillouin zones of each pair of layers; see Fig. 1(b). The positions of the corners of the three Brillouin zones are

$$\begin{aligned} \boldsymbol{K}_{G,top} &\approx \frac{4\pi}{3d_G}(\boldsymbol{n}_x + \theta_{TBG}\boldsymbol{n}_y), \quad \boldsymbol{K}_{G,bottom} = \frac{4\pi}{3d_G}\boldsymbol{n}_x, \\ \boldsymbol{K}_{hBN} &\approx \frac{4\pi}{3d_{hBN}}(\boldsymbol{n}_x - \theta_{hBN}\boldsymbol{n}_y) \\ &\approx \frac{4\pi}{3d_G}\left(1 - \frac{d_{hBN}}{d_G}\boldsymbol{n}_x - \theta_{hBN}\boldsymbol{n}_y\right), \end{aligned} \tag{1}$$

*These authors contributed equally.

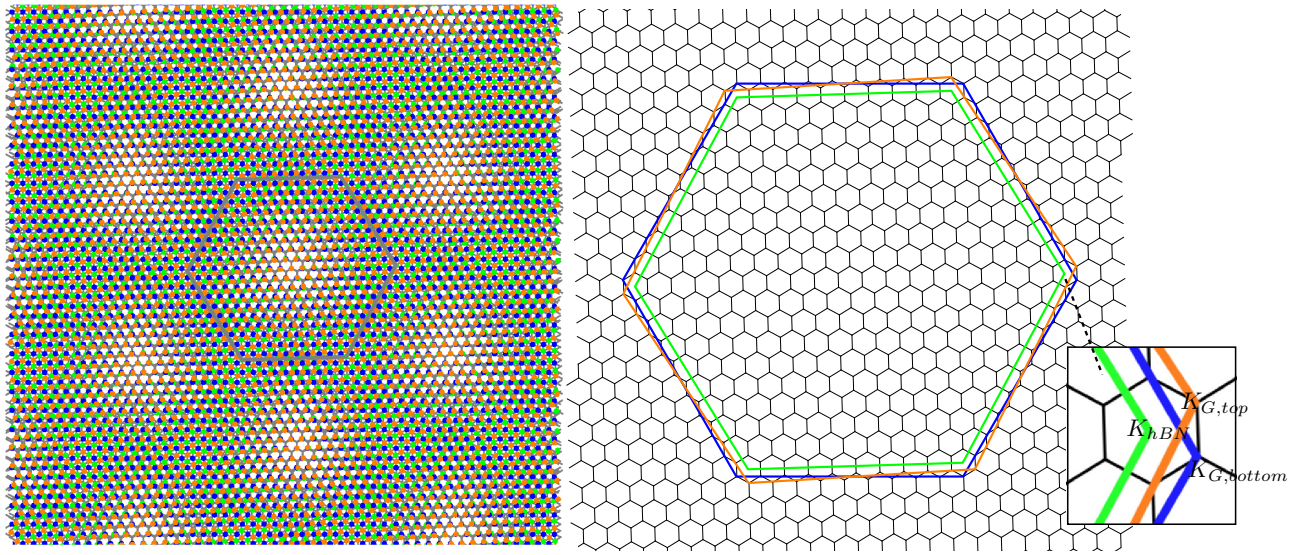

FIG. 1. (a) Sketch of the moiré superlattice. The blue and orange points represent the carbon atoms, while the green points refer to the substrate. (b) The large hexagons represent the BZs of the constituting layers. Their folding gives rise to the mini-BZs represented by the small black hexagons. In the inset: One side of the mini-BZ connects the corners of the BZs of each pair of layers.

where $\boldsymbol{n}_x$ and $\boldsymbol{n}_y$ are unit vectors along the x and y axes, and we have expanded the exact expressions to lowest order, $\theta_{TBG}, \theta_{hBN}, d_{hBN}/d_G - 1 \ll 1$. In order for the two moirés to have the same unit cell, we need the vectors $\boldsymbol{K}_{G,top} - \boldsymbol{K}_{G,bottom}$ and $\boldsymbol{K}_{G,top} - \boldsymbol{K}_{hBN}$ to have the same length, and to make an angle equal to $(2\pi)/3$. These two conditions imply that

$$\theta_{TBG} \approx \sqrt{\theta_{hBN}^2 + \left(\frac{d_{hBN}}{d_G} - 1\right)^2},$$
$$\frac{\theta_{hBN}}{\theta_{TBG}} = \frac{1}{2}. \tag{2}$$

For a fixed value of d_{hBN}/d_G these equations are satisfied when

$$\theta_{TBG} \approx 2\theta_{hBN} \approx \frac{2}{\sqrt{3}}\left(\frac{d_{hBN}}{d_G} - 1\right). \tag{3}$$

For $d_G = 2.46$ Å, $d_{hBN} = 2.50$ Å, and $d_{hBN}/d_G - 1 \approx 0.017$ we obtain $\theta_{TBG} \simeq 1.05^\circ$. This number is reasonably close to the twist angles where TBG shows a nontrivial phase diagram. The twist of hBN, $\theta_{hBN} \approx 0.52^\circ$, is close to perfect alignment. The presence of a unique moiré pattern in hBN/TBG heterostructures is consistent with recent scanning-tunneling-microscopy (STM) maps [12], where, in some samples, only the moiré pattern identified by the TBG appears.

III. RESULTS

We model the Hamiltonian of the TBG within the low energy continuum model, see [43–46], accounting for the lattice relaxation through the difference between the interlayer hoppings between the *AA* and the *AB* sublattices [46]. A detailed analysis of the lattice relaxation within the continuum model of the TBG can be found in [47]. The effect of the hBN is included by means of an effective periodic potential acting on the nearest graphene layer [31,48], which also accounts for the effects of lattice relaxation. In what follows we refer to the parametrization of such potential as given in the Ref. [49]. A detailed description of the model is given in the Supplemental Material [50].

We first study the arrangement described by the angles $\theta_{TBG} = 1.05^\circ$ and $\theta_{hBN} = 0.52^\circ$, where a single moiré unit cell describes the system, as shown in Fig. 1. Note that three different stacking configurations of the twisted system can be identified; see the Supplemental Material [50], Figs. S3 and S4. The three stackings differ in the relative arrangement of layers which are second-nearest neighbors. As shown below, the three geometries lead to different electronic structures.

The band structure and density of states (DOS) per unit cell of the hBN/TBG are shown in the Fig. 2 (black lines), and compared to that of the TBG (red dashed lines). $A_c = \sqrt{3}L_{TBG}^2/2$ is the area of the moiré unit cell. The presence of the substrate strongly affects the spectrum of the TBG. The flat bands at CN of the TBG become dispersive in the hBN/TBG stack, acquiring a finite bandwidth of ∼6–8 meV, which is almost twice that of the TBG. As a consequence, the peak in the DOS of the TBG at CN is strongly smoothed and also split in the hBN/TBG, giving rise to an insulating structure with a small band gap, which is due to the breaking of $\mathcal{C}_2$ induced by the hBN layer. This symmetry breaking also gives rise to a finite Berry curvature whose integral in the mini-BZ results in the valley Chern numbers (see the Supplemental Material [50]) indicated in each panel of Fig. 2. The effect of a self-consistent Hartree potential away from CN is shown in Figs. 3 and 4, where even with smoothed peaks in the DOS, the Fermi level is quite close to the van Hove singularities [51]. The Chern numbers of these bands are shown in the Supplemental Material [50]. It is worth mentioning that Chern numbers of up to $\mathcal{C} = 3$ are obtained. The effect of the exchange term at the neutrality point is analyzed in the Supplemental Material [50]. As in the absence of a substrate [51,52], the bands are significantly distorted by the Hartree potential.

Generic values of the twist angle between hBN and TBG cannot be described by a simple moiré unit cell. This is, for

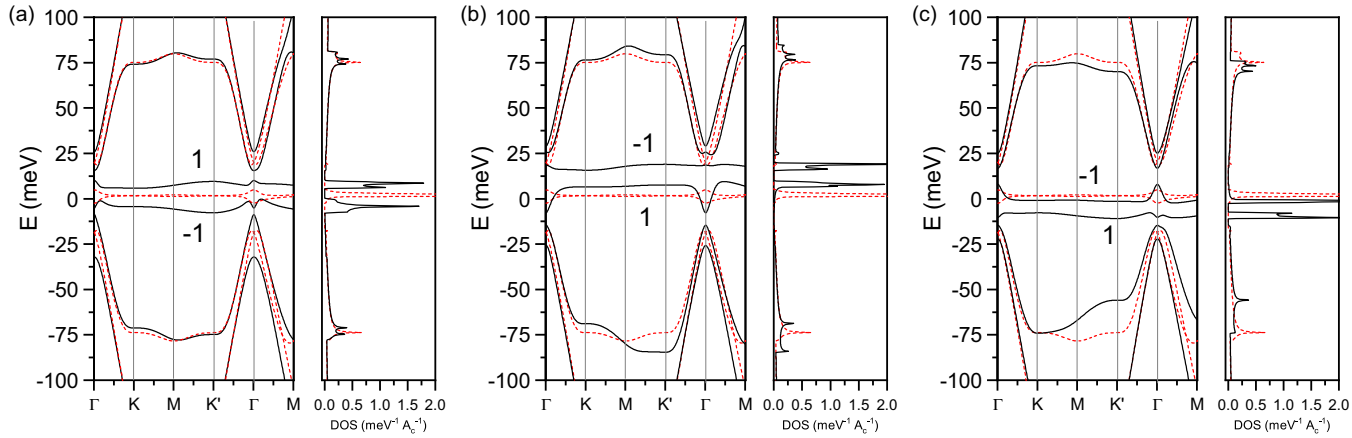

FIG. 2. Band structure of TBG on top of hBN for (a) *AAA*, (b) *CAA*, and (c) *BAA* stacking. The red dashed lines show the energy bands and DOS of the TBG decoupled from the substrate. The bands are computed in the K valley and the corresponding Chern numbers are provided. The Chern numbers of the K' valley have opposite sign.

example, the case for perfect alignment: $\theta_{hBN} = 0°$. Because of the lack of commensuration, we cannot define a crystal momentum. In order to study the energy spectrum, we project the perturbation induced by the hBN on the low-energy states of the TBG and solve a dual lattice in the reciprocal space of the TBG, as detailed in the Supplemental Material [50]. The scheme follows closely continuum models for a graphene monolayer on hBN, where the perturbation due to the hBN layer is projected onto the graphene Dirac cone. An infinite number of minibands emerge, induced by the periodicity of the potential due to the hBN layer. In a similar manner, the TBG bands are replicated and coupled in our calculation. A similar method has been recently used in the Ref. [53] for studying the quasicrystalline electronic spectrum of the noncommensurate 30° TBG.

The quasi-band-structures, obtained by varying the momentum $\boldsymbol{k}$ in the BZ of the TBG, and the DOS are shown in the Fig. 5 for different orientations between the hBN and graphene, and $\theta_{TBG} = 1.05°$. The black and red hexagons show the two different BZs of the TBG and of the hBN/G, respectively. The red lines refer to the band structure and the DOS of the unperturbed TBG, which also includes the long-wavelength staggered potential induced by the hBN, weakly breaking the C_2 symmetry of graphene (see the Supplemental Material [50]). As is evident, the hBN strongly affects the spectrum close to CN at small angles, $\theta_{hBN} < 1°$, where the moiré identified by the TBG and that identified by the substrate of hBN have similar periods. In contrast to the narrow bands of the TBG, the hBN/TBG exhibits a broad structure, with a bandwidth of approximatively 30 meV, which can even overlap with the higher energy bands. This is for example the case of $\theta_{hBN} = 0.52°$, Fig. 5(b), which is close to commensuration. In addition, the band broadening at CN lowers the DOS of the hBN/TBG as compared to the sharp van Hove singularity of the TBG, which has been cut out of the energy

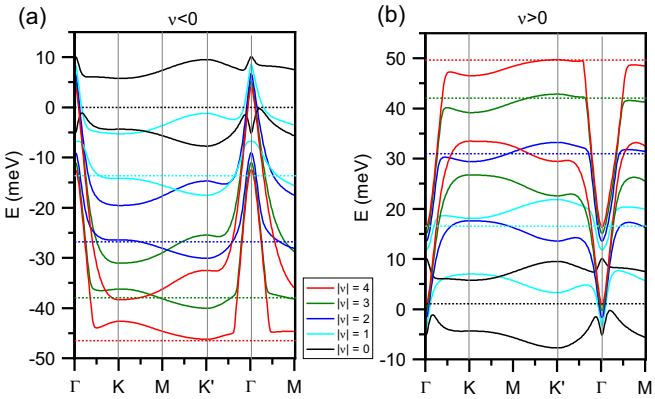

FIG. 3. Self-consistent bands of *AAA*-stacked hBN/TBG obtained for (a) negative and (b) positive filling. The horizontal dashed lines represent the Fermi energies.

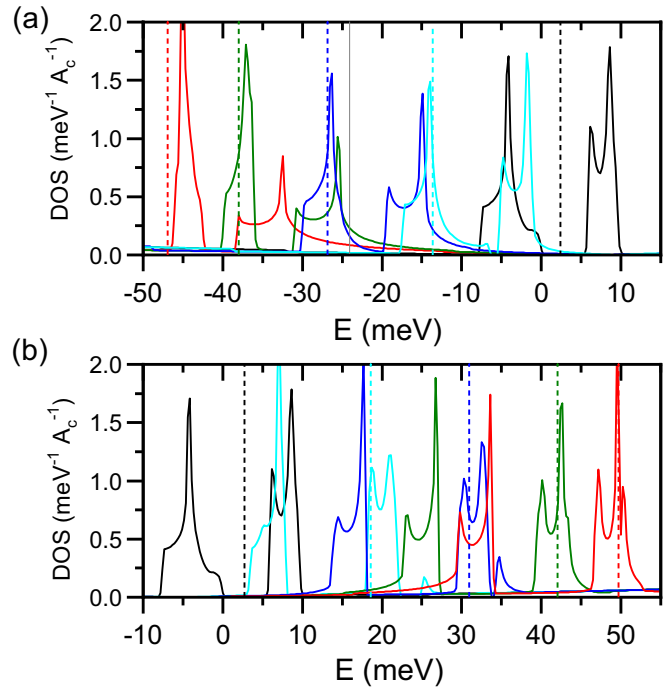

FIG. 4. DOS corresponding to the bands shown in Fig. 3 for (a) negative and (b) positive filling. The vertical dashed lines represent the Fermi energies.

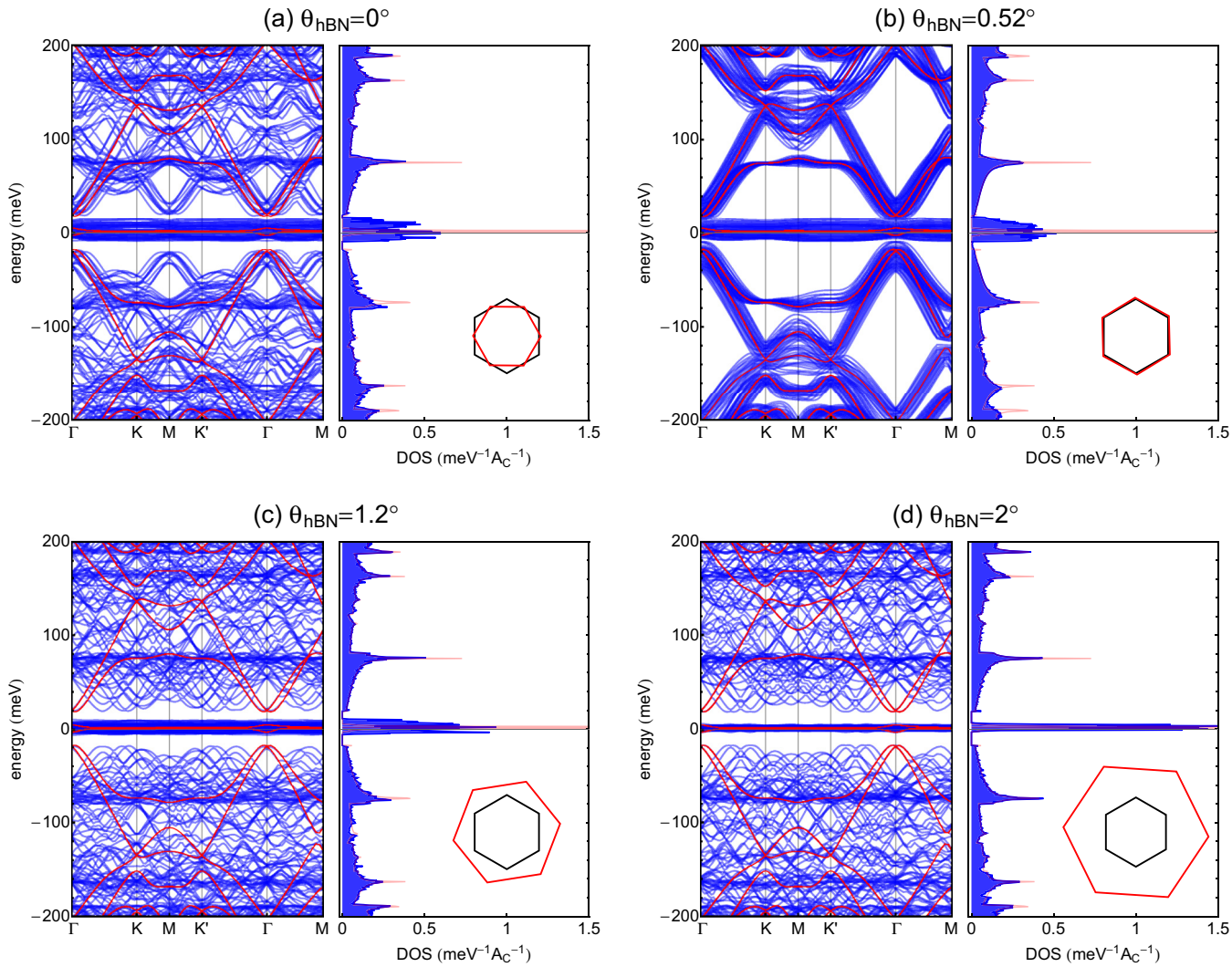

FIG. 5. Quasi-band-structure and DOS of the noncommensurate hBN/TBG. The black and red hexagons show the two different BZs of the TBG and of the hBN/G, respectively. The red lines refer to the band structure and the DOS of the unperturbed TBG.

scale in the central panels of Fig. 5. In general, the high-energy spectrum is barely affected by the hBN. Upon increasing θ_{hBN}, the bandwidth at CN gradually shrinks, while the DOS gains intensity and the central bands further separate from the rest of the spectrum. At $\theta_{hBN} = 2^\circ$ the effect of the hBN is almost completely negligible and we recover the narrow-band feature of the TBG, except for a constant gap. Even though we are using a small value of the staggered potential, $\Delta = 3.62$ meV, as given by Ref. [49], we checked that our results remain valid in a wide range of values of Δ. The details are shown in the Supplemental Material [50], where we report the case of $\Delta = 40$ meV.

It is worth noting that bandwidths of the order of 10–30 meV, like those reported here, are comparable to the electrostatic interactions. On the other hand, the smoothing of the DOS induced by the substrate is expected to reduce the role of the electronic interactions as compared to the case of the TBG decoupled by the substrate.

Finally, we show plots of the changes in the charge density distribution induced by the substrate in the Supplemental Material [50]. The sixfold symmetry of the TBG is reduced to threefold, in the case where the two moirés coincide. We expect a lower symmetry in the general case. These results are in agreement with the reduced symmetry observed in STM experiments [54].

IV. CONCLUSIONS

We have analyzed the effect of a nearly aligned hBN substrate on the low-energy bands of a TBG. We find the existence of *two* regimes: (i) For large angles, $\theta_{hBN} \gtrsim 2^\circ$, the TBG is effectively decoupled from the substrate, and only the average gap due to the breaking of inversion symmetry needs to be taken into account. (ii) For small angles, $\theta_{hBN} \lesssim 2^\circ$, the periodic potential with zero average over the unit cell induced by the substrate significantly alters the DOS, so that a model based on flat bands does not describe adequately the system. In this regime, the van Hove singularities are smoothed out, and the width of the peak near the Dirac energy increases from $W \sim 5$–10 meV for a decoupled TBG to $W \gtrsim 20$–30 meV for a well-aligned hBN/TBG stack. This peak overlaps with higher energy bands. In addition, the gap expected from the lack of inversion symmetry becomes filled with states which

arise from the nonuniform part of the perturbation due to the substrate.

In a counterintuitive fashion, the effect of the alignment between TBG and the substrate is similar to the effect of strong disorder on the flat bands. Subtle features, such as van Hove singularities, will be suppressed. Presumably, Shubnikov–de Haas oscillations and Landau levels at low magnetic fields will be suppressed as well.

ACKNOWLEDGMENTS

This work was supported by funding from the European Commission, under the Graphene Flagship, Core 3, Grant No. 881603, and by the grants NMAT2D (Comunidad de Madrid, Spain) and SprQuMat and SEV-2016-0686 (Ministerio de Ciencia e Innovación, Spain).

[1] Y. Cao, V. Fatemi, A. Demir, S. Fang, S. L. Tomarken, J. Y. Luo, J. D. Sanchez-Yamagishi, K. Watanabe, T. Taniguchi, E. Kaxiras, R. C. Ashoori, and P. Jarillo-Herrero, Correlated insulator behavior at half-filling in magic-angle graphene superlattices, Nature (London) **556**, 80 (2018).

[2] Y. Cao, V. Fatemi, S. Fang, K. Watanabe, T. Taniguchi, E. Kaxiras, and P. Jarillo-Herrero, Unconventional superconductivity in magic-angle graphene superlattices, Nature (London) **556**, 43 (2018).

[3] K. Kim, A. DaSilva, S. Huang, B. Fallahazad, S. Larentis, T. Taniguchi, K. Watanabe, B. J. LeRoy, A. H. MacDonald, and E. Tutuc, Tunable moiré bands and strong correlations in small-twist-angle bilayer graphene, Proc. Natl. Acad. Sci. USA **114**, 3364 (2017).

[4] S. Huang, K. Kim, D. K. Efimkin, T. Lovorn, T. Taniguchi, K. Watanabe, A. H. MacDonald, E. Tutuc, and B. J. LeRoy, Topologically Protected Helical States in Minimally Twisted Bilayer Graphene, Phys. Rev. Lett. **121**, 037702 (2018).

[5] M. Yankowitz, S. Chen, H. Polshyn, Y. Zhang, K. Watanabe, T. Taniguchi, D. Graf, A. F. Young, and C. R. Dean, Tuning superconductivity in twisted bilayer graphene, Science **363**, 1059 (2019).

[6] X. Lu, P. Stepanov, W. Yang, M. Xie, M. A. Aamir, I. Das, C. Urgell, K. Watanabe, T. Taniguchi, G. Zhang, A. Bachtold, A. H. MacDonald, and D. K. Efetov, Superconductors, orbital magnets and correlated states in magic-angle bilayer graphene, Nature (London) **574**, 653 (2019).

[7] S. L. Tomarken, Y. Cao, A. Demir, K. Watanabe, T. Taniguchi, P. Jarillo-Herrero, and R. C. Ashoori, Electronic Compressibility of Magic-Angle Graphene Superlattices, Phys. Rev. Lett. **123**, 046601 (2019).

[8] A. L. Sharpe, E. J. Fox, A. W. Barnard, J. Finney, K. Watanabe, T. Taniguchi, M. A. Kastner, and D. Goldhaber-Gordon, Emergent ferromagnetism near three-quarters filling in twisted bilayer graphene, Science **365**, 605 (2019).

[9] P. Stepanov, I. Das, X. Lu, A. Fahimniya, K. Watanabe, T. Taniguchi, F. H. L. Koppens, J. Lischner, L. Levitov, and D. K. Efetov, The interplay of insulating and superconducting orders in magic-angle graphene bilayers, Nature **583**, 375 (2020).

[10] U. Zondiner, A. Rozen, D. Rodan-Legrain, Y. Cao, R. Queiroz, T. Taniguchi, K. Watanabe, Y. Oreg, F. von Oppen, A. Stern, E. Berg, P. Jarillo-Herrero, and S. Ilani, Cascade of phase transitions and Dirac revivals in magic angle graphene, Nature (London) **582**, 203 (2020).

[11] Y. Xie, B. Lian, B. Jäck, X. Liu, C. L. Chiu, K. Watanabe, T. Taniguchi, B. A. Bernevig, and A. Yazdani, Spectroscopic signatures of many-body correlations in magic-angle twisted bilayer graphene, Nature (London) **572**, 101 (2019).

[12] D. Wong, K. P. Nuckolls, M. Oh, B. Lian, Y. Xie, S. Jeon, K. Watanabe, T. Taniguchi, B. A. Bernevig, and A. Yazdani, Cascade of electronic transitions in magic-angle twisted bilayer graphene, Nature (London) **582**, 198 (2020).

[13] H. Singh Arora, R. Polski, Y. Zhang, A. Thomson, Y. Choi, H. Kim, Z. Lin, I. Zaky Wilson, X. Xu, J.-H. Chu, K. Watanabe, T. Taniguchi, J. Alicea, and S. Nadj-Perge, Superconductivity without insulating states in twisted bilayer graphene stabilized by monolayer WSe_2, Nature (London) **583**, 379 (2020).

[14] B. Hunt, J. D. Sanchez-Yamagishi, A. F. Young, M. Yankowitz, B. J. LeRoy, K. Watanabe, T. Taniguchi, P. Moon, M. Koshino, P. Jarillo-Herrero, and R. C. Ashoori, Massive Dirac fermions and Hofstadter butterfly in a van der Waals heterostructure, Science **340**, 1427 (2013).

[15] J. C. W. Song, A. V. Shytov, and L. S. Levitov, Electron Interactions and Gap Opening in Graphene Superlattices, Phys. Rev. Lett. **111**, 266801 (2013).

[16] F. Amet, J. R. Williams, K. Watanabe, T. Taniguchi, and D. Goldhaber-Gordon, Insulating Behavior at the Neutrality Point in Single-Layer Graphene, Phys. Rev. Lett. **110**, 216601 (2013).

[17] R. V. Gorbachev, J. Song, G. L. Yu, A. V. Kretinin, F. Withers, Y. Cao, A. Mishchenko, I. V. Grigorieva, K. S. Novoselov, L. S. Levitov, and A. K. Geim, Detecting topological currents in graphene superlattices, Science **346**, 448 (2014).

[18] Z.-G. Chen, Z. Shi, W. Yang, X. Lu, Y. Lai, H. Yan, F. Wang, G. Zhang, and Z. Li, Observation of an intrinsic bandgap and Landau level renormalization in graphene/boron-nitride heterostructures, Nat. Commun. **5**, 4461 (2014).

[19] M. Yankowitz, J. Xue, and B. J. LeRoy, Graphene on hexagonal boron nitride, J. Phys.: Condens. Matter **26**, 303201 (2014).

[20] D. Wong, Y. Wang, J. Jung, S. Pezzini, A. M. DaSilva, H.-Z. Tsai, H. S. Jung, R. Khajeh, Y. Kim, J. Lee, S. Kahn, S. Tollabimazraehno, H. Rasool, K. Watanabe, T. Taniguchi, A. Zettl, S. Adam, A. H. MacDonald, and M. F. Crommie, Local spectroscopy of moiré-induced electronic structure in gate-tunable twisted bilayer graphene, Phys. Rev. B **92**, 155409 (2015).

[21] J. Jung, A. M. Dasilva, A. H. MacDonald, and S. Adam, Origin of band gaps in graphene on hexagonal boron nitride, Nat. Commun. **6**, 6308 (2015).

[22] M. Lee, J. R. Wallbank, P. Gallagher, K. Watanabe, T. Taniguchi, V. I. Fal'ko, and D. Goldhaber-Gordon, Ballistic miniband conduction in a graphene superlattice, Science **353**, 1526 (2016).

[23] E. Wang, X. Lu, S. Ding, W. Yao, M. Yan, G. Wan, K. Deng, S. Wang, G. Chen, L. Ma, J. Jung, A. V. Fedorov, Y. Zhang, G. Zhang, and S. Zhou, Gaps induced by inversion symmetry breaking and second-generation Dirac cones in graphene/hexagonal boron nitride, Nat. Phys. **12**, 1111 (2016).

[24] M. Yankowitz, J. Jung, E. Laksono, N. Leconte, B. L. Chittari, K. Watanabe, T. Taniguchi, S. Adam, D. Graf, and C. R. Dean, Dynamic band-structure tuning of graphene moiré superlattices with pressure, Nature (London) **557**, 404 (2018).

[25] A. A. Zibrov, E. M. Spanton, H. Zhou, C. Kometter, T. Taniguchi, K. Watanabe, and A. F. Young, Even-denominator fractional quantum Hall states at an isospin transition in monolayer graphene, Nat. Phys. **14**, 930 (2018).

[26] H. Kim, N. Leconte, B. L. Chittari, K. Watanabe, T. Taniguchi, A. H. Macdonald, J. Jung, and S. Jung, Accurate gap determination in monolayer and bilayer graphene/h-BN moiré superlattices, Nano Lett. **18**, 7732 (2018).

[27] J. Xue, J. Sanchez-Yamagishi, D. Bulmash, P. Jacquod, A. Deshpande, K. Watanabe, T. Taniguchi, P. Jarillo-Herrero, and B. J. LeRoy, Scanning tunneling microscopy and spectroscopy of ultra-flat graphene on hexagonal boron nitride, Nat. Mater. **10**, 282 (2011).

[28] M. Yankowitz, J. Xue, D. Cormode, J. D. Sanchez-Yamagishi, K. Watanabe, T. Taniguchi, P. Jarillo-Herrero, P. Jacquod, and B. J. LeRoy, Emergence of superlattice Dirac points in graphene on hexagonal boron nitride, Nat. Phys. **8**, 382 (2012).

[29] C. R. Woods, L. Britnell, A. Eckmann, R. S. Ma, J. C. Lu, H. M. Guo, X. Lin, G. L. Yu, Y. Cao, R. V. Gorbachev, A. V. Kretinin, J. Park, L. A. Ponomarenko, M. I. Katsnelson, Y. N. Gornostyrev, K. Watanabe, T. Taniguchi, C. Casiraghi, H.-J. Gao, A. K. Geim, and K. S. Novoselov, Commensurate-incommensurate transition in graphene on hexagonal boron nitride, Nat. Phys. **10**, 451 (2014).

[30] P. Moon and M. Koshino, Electronic properties of graphene/hexagonal-boron-nitride moiré superlattice, Phys. Rev. B **90**, 155406 (2014).

[31] P. San-Jose, A. Gutiérrez-Rubio, M. Sturla, and F. Guinea, Spontaneous strains and gap in graphene on boron nitride, Phys. Rev. B **90**, 075428 (2014).

[32] Y.-H. Zhang, D. Mao, and T. Senthil, Twisted bilayer graphene aligned with hexagonal boron nitride: Anomalous Hall effect and a lattice model, Phys. Rev. Res. **1**, 033126 (2019).

[33] N. Bultinck, S. Chatterjee, and M. P. Zaletel, Mechanism for Anomalous Hall Ferromagnetism in Twisted Bilayer Graphene, Phys. Rev. Lett. **124**, 166601 (2020).

[34] M. Serlin, C. L. Tschirhart, H. Polshyn, Y. Zhang, J. Zhu, K. Watanabe, T. Taniguchi, L. Balents, and A. F. Young, Intrinsic quantized anomalous Hall effect in a moiré heterostructure, Science **367**, 900 (2020).

[35] J. Slawińska, I. Zasada, P. Kosiński, and Z. Klusek, Reversible modifications of linear dispersion: Graphene between boron nitride monolayers, Phys. Rev. B **82**, 085431 (2010).

[36] N. Bultinck, E. Khalaf, S. Liu, S. Chatterjee, A. Vishwanath, and M. P. Zaletel, Ground State and Hidden Symmetry of Magic Angle Graphene at Even Integer Filling, Phys. Rev. X **10**, 031034 (2020).

[37] E. Khalaf, S. Chatterjee, N. Bultinck, M. P. Zaletel, and A. Vishwanath, Charged skyrmions and topological origin of superconductivity in magic angle graphene, arXiv:2004.00638.

[38] B. Amorim and E. V. Castro, Electronic spectral properties of incommensurate twisted trilayer graphene, arXiv:1807.11909.

[39] C. Mora, N. Regnault, and B. A. Bernevig, Flatbands and Perfect Metal in Trilayer Moiré Graphene, Phys. Rev. Lett. **123**, 026402 (2019).

[40] T. Cea, N. R. Walet, and F. Guinea, Twists and the electronic structure of graphitic materials, Nano Lett. **19**, 8683 (2019).

[41] T. Cea and F. Guinea, Band Structure and Insulating States Driven by the Coulomb Interaction in Twisted Bilayer Graphene, Phys. Rev. B **102**, 045107 (2020).

[42] P. A. Pantaleon, T. Cea, R. Brown, N. R. Walet, and F. Guinea, Narrow bands and electrostatic interactions in graphene stacks, arXiv:2003.05050.

[43] J. M. B. Lopes dos Santos, N. M. R. Peres, and A. H. Castro Neto, Graphene Bilayer with a Twist: Electronic Structure, Phys. Rev. Lett. **99**, 256802 (2007).

[44] R. Bistritzer and A. H. MacDonald, Moiré bands in twisted double-layer graphene, Proc. Natl. Acad. Sci. USA **108**, 12233 (2011).

[45] J. M. B. Lopes dos Santos, N. M. R. Peres, and A. H. Castro Neto, Continuum model of the twisted graphene bilayer, Phys. Rev. B **86**, 155449 (2012).

[46] M. Koshino, N. F. Q. Yuan, T. Koretsune, M. Ochi, K. Kuroki, and L. Fu, Maximally Localized Wannier Orbitals and the Extended Hubbard Model for Twisted Bilayer Graphene, Phys. Rev. X **8**, 031087 (2018).

[47] F. Guinea and N. R. Walet, Continuum models for twisted bilayer graphene: Effect of lattice deformation and hopping parameters, Phys. Rev. B **99**, 205134 (2019).

[48] J. R. Wallbank, A. A. Patel, M. Mucha-Kruczyński, A. K. Geim, and V. I. Fal'ko, Generic miniband structure of graphene on a hexagonal substrate, Phys. Rev. B **87**, 245408 (2013).

[49] J. Jung, E. Laksono, A. M. DaSilva, A. H. MacDonald, M. Mucha-Kruczyński, and S. Adam, Moiré band model and band gaps of graphene on hexagonal boron nitride, Phys. Rev. B **96**, 085442 (2017).

[50] See Supplemental Material at http://link.aps.org/supplemental/10.1103/PhysRevB.102.155136 for Geometry of the superlattice; The continuum model of the TBG; The continuum model of the commensurate heterostructures hBN/TBG and hBN/TBG/hBN; Topological phases induced by the Hartree potential; Changes in the charge density induced by the substrate; Hartree-Fock band structure of the commensurate hBN/TBG; The case of non-commensurate heterostructures of hBN/TBG.

[51] T. Cea, N. R. Walet, and F. Guinea, Electronic band structure and pinning of Fermi energy to Van Hove singularities in twisted bilayer graphene: A self-consistent approach, Phys. Rev. B **100**, 205113 (2019).

[52] F. Guinea and N. R. Walet, Electrostatic effects, band distortions, and superconductivity in twisted graphene bilayers, Proc. Natl. Acad. Sci. **115**, 13174 (2018).

[53] P. Moon, M. Koshino, and Y.-W. Son, Quasicrystalline electronic states in 30° rotated twisted bilayer graphene, Phys. Rev. B **99**, 165430 (2019).

[54] Y. Jiang, J. Mao, X. Lai, K. Watanabe, T. Taniguchi, K. Haule, and E. Y. Andrei, Charge-order and broken rotational symmetry in magic angle twisted bilayer graphene, Nature (London) **573**, 91 (2019).